

Red shift effect on the zero field splitting for negatively charged nitrogen-vacancy centers in diamond

Wang Zheng^{1,2}, Zhang Jintao^{2,*}, Feng Xiaojuan², Xing Li²

¹ *Department of Precision Instruments, Tsinghua University, Beijing, China*

² *Division of Thermophysics Metrology, National Institute of Metrology, Beijing, China*

The zero field splitting (ZFS) quantifies the energy difference of the ground electron spin-triplet of a NV^- center in the absence of external fields. The values of the ZFS play the centrality for determination of the Larmor precession of the Bloch sphere and the Rabi oscillation of the spin system. A coherent spin manipulation by sweeping microwave (MW) at frequencies near the resonance with the ZFS is a general method detecting ZFS. We reported in this letter our experimental observation of the red shift effect on the ZFS as a function of MW power for two different thermal environments of the sample. We find the asymptotic property of the red shifts of the ZFS. Giving the identical initial thermal equilibrium state of the sample, the differences of the raw values of the ZFS between the two cases randomly vary in 47 kHz to 1505 kHz in the entire experimental range. By the asymptotic approximation, the differences are suppressed into 29 kHz to 166 kHz with the standard deviation of 49 kHz, suggesting a significant elimination of the red shift effect. To our knowledge, no report has yet addressed the quantification and elimination of the red shift effect of the MW field dependence by the asymptotic approximation before this work.

A nitrogen vacancy (NV) color center is a unique point defect in diamond consisting of a substitutional nitrogen atom adjacent to a vacancy within the rigid lattice. The symmetry axis of each NV center is along one of the four (111) crystalline direction. The geometric structure of a NV^- color center is pictured in Fig. 1(a). The negatively charged center (NV^-) has the spin-triplet ground state ($S = 1$), the $|m_s=0\rangle$ and the degenerate $|m_s=\pm 1\rangle$, of the ZFS, denoted as D , due to spin-spin interactions. The ZFS is sensitive to magnetic fields, electric fields, lattice strains and temperatures, allowing NV^- center as a multimodal sensor of high spatial resolution [1]. As shown in Fig. 1(b), the transition of the ground state and the excitation state is of the energy level of 1.945 eV (corresponding to a zero phonon line wavelength of 637 nm). Upon the spin-conserving optical excitation, the spin-triplet ground state can be initialized to $|m_s=0\rangle$, because the electrons in $|m_s=\pm 1\rangle$ of the excited state more likely undergo inter-system crossing (ISC) to $|m_s=0\rangle$ of the ground state via the associated singlet states [1]. Accordingly, the population in the $|m_s=0\rangle$ state results in higher fluorescence under optical excitation than the population in the $|m_s=\pm 1\rangle$ state because of the spin polarization via ISC. A coherent spin manipulation of the ground spin triplet by sweeping microwave frequencies near the resonance with the ZFS can make prominent photo luminescence contrast for the spin-state-dependent fluorescence, giving the ZFS optically readout, a process called by the optically detected magnetic resonance (ODMR) [4]. A number of studies have demonstrated the dependence of the ZFS on the temperature and the strain of the crystal lattices hosting the NV centers. Given zero strain effect, a NV^- center in diamond play the temperature sensor. Acosta, et al.

* zhangjint@nim.ac.cn

demonstrate the temperature measurement by probing the shift of the ZFS using ODMR [5]. Kusko, et al. demonstrated the resolution of 0.1 K in a dimension of 200 nm [6]. Toyli, et al. demonstrated the temperature sensor using single NV⁻ center up to 600 K [7]. The high spatial resolution and biocompatibility make NV⁻ centers in diamond the promising temperature sensors for living cells [8].

The ZFS, the critical parameter determining the Larmor precession of the Bloch sphere, bases the core of the ODMR scheme[1]. The resonance with the ZFS is the basis of the Rabi oscillation. The protocol of the Ramsey interference and the pulsed ODMR (p-ODMR), based on the Rabi frequency and the Larmor precession of the Bloch sphere, is the principal method for elimination of the dephasing effect arising from static and slowly varying inhomogeneities, e.g., dipolar fields of spin impurities in the diamond sample [15]. These dynamical decoupling protocols extend the spin coherence lifetime for longer phase memory [7]. When a detuning of the ZFS is present, the Rabi frequency will need to be replaced by the effective Rabi frequency [17]. The sensitivity of spin readout will be degraded. Besides, Guillebon, et al. stated that the longitudinal spin relaxation time of a NV⁻ center is shortened by heating the diamond lattice [18]. Such temperature dependence degrades the detection sensitivity of magnetic fields via quantum lock-in [19].

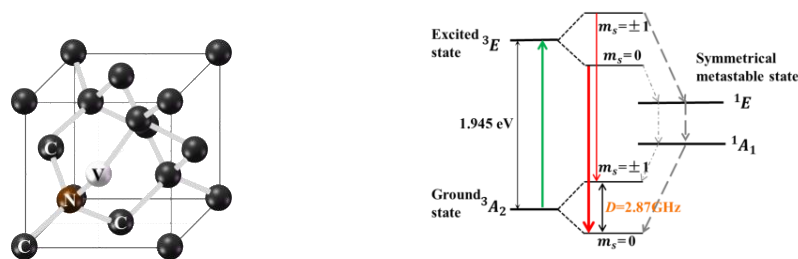


Fig. 1 (a)Geometric structure of NV center. (b)Energy level structure of NV center.

The ISC for polarization of spin state via the ODMR scheme causes the red shifts of the ZFS because the electron-phonon interaction emits phonons heating the diamond lattice [20]. We and others have experimentally observed the laser heating effect on NV⁻ centers in diamond [21]. Besides, the microwave (MW) irradiation for manipulation of the spin triplet state imposes heating to the diamond sample. We have reported our quantitative investigation on the microwave heating effect associating with ODMR [24]. We observed that the microwave heating effect, more significant than the laser, depends on MW power. Fujiwara, et al. stated their observation that, when measuring the temperatures of biological samples using NV⁻ centers in diamond, microwave irradiation can cause a change in the temperature during the measurement process because of microwave-induced water heating, resulting in a ZFS shift [25]. Lillie, *et al.* detected temperature changes in the sample by a thermistor when only microwave was turned on, and found the presence of microwave heating [21]. Wang *et al.* discovered that the input of microwaves would affect the environmental temperatures of diamonds, and quantitatively measured their local temperature changes [26].

Thus, a thorough understanding of the red shift effect on the ZFS by MW fields is of the fundamental importance for the theoretical modeling of the ZFS and the metrology using NV⁻ centers as a nanothermometer, magnetometer, etc. We are motivated to study the quantification and elimination of the red shift effect on the ZFS of the MW field dependence. We reported in this paper our experimental study on the ensemble NV⁻ centers driven by the continuous-wave ODMR (cw-ODMR) scheme. The scheme has the advantage of the experimental simplicity and

the tolerance of MW inhomogeneities, thus is widely employed for metrology using NV⁻ centers. The measurements by the scheme have desired sensitivities when a large ensemble NV⁻ centers are interrogated with the same optical excitation power [6,11,27,28]. We conducted the study for two different thermal environments with the diamond sample, Case I specific for constant current heating the diamond sample to reach a desired temperature, Case II for proportional integral derivative (PID) controlling the temperature of diamond sample. We find the red shifts of the ZFS obeying the asymptotic dependence of MW fields. We demonstrate the significant elimination of the red shift effect by extraction of the values of the ZFS at zero MW field through the asymptotic approximation.

We schematically diagrammed the experiment setup in Fig. 2(a) for the protocol of cw-ODMR. The setup composes of the confocal optical path for the photoluminescence of NV⁻ centers and the fluorescence collection, and the microwave driving facility. A 532 nm laser (MGL-III-532nm, output power > 200 mW, power stability <1% (rms, over 4 hours)) is directed towards the diamond sample through the confocal optical path. We use an acousto-optic modulator (AOM, G&H AOM3350-199) as the switch for the laser, and use an aperture to select the first-order diffraction light modulated by the AOM for subsequent excitation of the sample. Then, the laser is reflected by the dichroic mirror (DMLP550R) to the objective lens (Olympus, UPLSAPO60XO) and directed towards the sample. The NV⁻ centers undergoing photoluminescence generate fluorescence around 637 nm, which is collected by the confocal optical path, filtered and focused into a multimode fiber for detection by a single photon counting modulator (SPCM-AQRH-11-FC). The outputs of the detector are acquired by the computer via a data acquisition card (DAQ, PXIe-6363). The MWs are generated by Stanford Research System SG386 and transmitted to an amplifier (Mini-Circuits, ZHL-16W-43-S+) via a radio frequency microwave switch (Mini-Circuits, ZASWA-2-50DRA+), and finally transmitted to the vicinity of the diamond sample by a 60 μ m copper wire antenna laid on the gold-plated printed circuit board (PCB). The PCB board is connected to a 50 Ω impedance resistor absorbing excess MWs for prevention of reflection signals of MWs interfering and damaging the instruments. The bulk diamond sample is provided by Element Six which is made of chemical vapor deposition (CVD) synthesis and the size is 2.6 mm \times 2.6 mm \times 0.3 mm. As is shown in Fig. 2(b), the sample is bonded to a glass slide, which is bonded to the upper surface of the PCB board, and the back surface of the glass slide is attached by a film heater of polyimide.

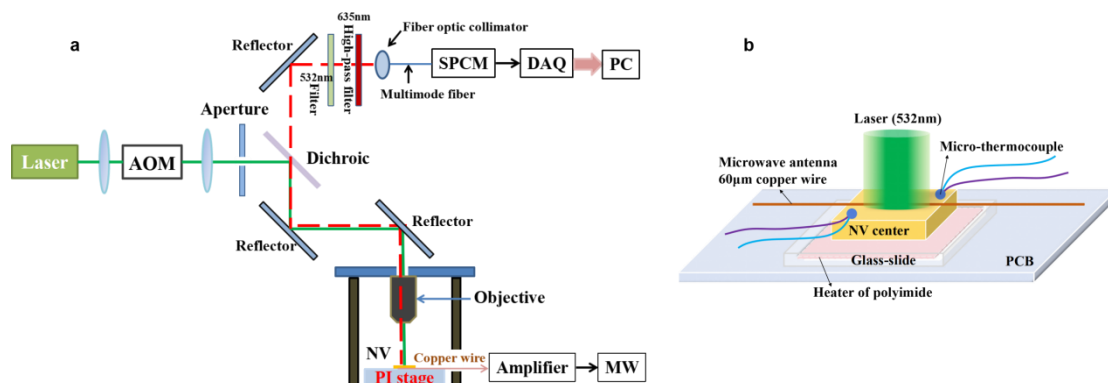


FIG. 2. Schematic diagram of experimental system. (a) Laser illuminating system. (b) diagram for MW antenna and thermopile.

We constructed a thermopile by connecting two K-type sheathed thermocouples in series. The wires of the thermocouples are 0.127 mm in diameter. The reference elements of the thermopile were maintained in a cell of the triple point of water (TPW) that is 273.16 K. The TPW cell demonstrated a temperature difference of 0.05 mK from the primary standard of the National Institute of Metrology (NIM), China. The two probing ends of the thermopile were diagonally attached on the edge of the diamond sample, and the reference ends of the thermopile were accommodated in the cell of TPW. The entire diamond sample was wrapped by thermal insulator.

In order to suppress the noises arising from the optical excitation and readout, we took the modified protocol of cw-ODMR that we published previously [23]. We pictured the protocol in Fig. 3. The MWs were programmed into a sequence of identical interval pulses, while the laser kept irradiation in the whole round of measurement. This scheme compares the photoluminescence fluorescence of the NV⁻ centers with and without microwave irradiation to depress the effect of noises arising from laser irradiation. We selected an interval of 5 ms for our measurements. We use a pulse signal generator to achieve synchronization and control of microwave pulses and fluorescence collection. The MWs were swept in the frequencies ranging from 2850 MHz to 2980 MHz of a step of 0.5 MHz. A microwave pulse was applied in 5 ms with a synchronizing photon counting. An extra photon counting was applied in 5 ms in the absence of MW pulse. The pulsing processes were circulated in 300 times to finish measurement of a single step of MWs.

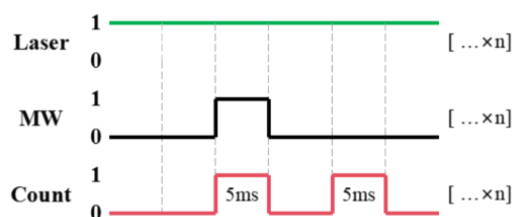


FIG. 3. Time sequences of the cw-ODMR.

As stated above, we designed two cases for the thermal environments of the sample. For Case I, we applied a constant current into the film heater to achieve a desired stationary temperature through the diamond sample. The total length obtaining an entire ODMR line was in 160 s. During the period, the temperature fluctuation was maintained within ± 0.05 K. For Case II, we applied a PID regulation of the power of the film heater for a desired temperature. The temperature fluctuation was controlled within ± 0.02 K. We conducted the study in the nominal sample temperatures ranging from 298.15 K to 323.15 K in an interval of 5 K. The MWs for manipulation of the spin system were selected in the power of -25 dBm, -20 dBm, -15 dBm, -11 dBm, -10 dBm, -5 dBm, 0 dBm and 5 dBm and 6 dBm. The laser radiation for optical excitation maintained a constant power of 3.96 mW.

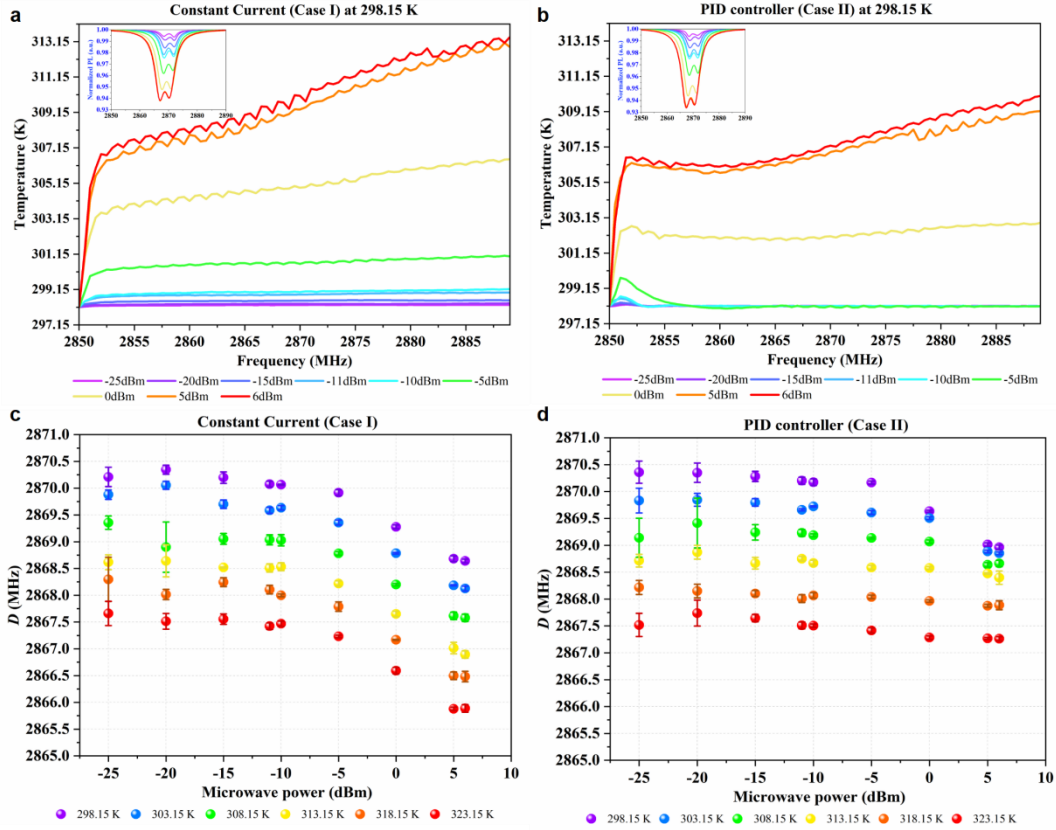


FIG. 4. (a, b) Diamond sample temperatures of the MW field dependence, and the inset of the respective ODMR lines. (c, d) Plots of the red shifts of the ZFS of the MW field dependence.

We diagrammed in Fig. 4(a) and 4(b) the sample temperature variations and the ODMR lines of the MW power dependence for Case I and II of the initial sample temperature at 298.15 K. In Fig. 4(a) the results of Case I illustrate the unified rises of the sample temperatures with the MW powers. The sample temperatures rise rapidly at the first 10 seconds after the MW irradiation, then, slowly during the subsequent times. The minimum temperature rise was in 0.13 K at the MW power of -25 dBm and the maximum was in 15.4 K at 6 dBm. The ODMR lines display increasing contrast and broadening.

In Fig. 4(b) the results of Case II show a threshold of MW power existing for sample temperature variations. For a MW power below the threshold, the sample temperature rapidly rises after the microwave irradiation is turned on, and then are quickly converged in decaying oscillations to the original sample temperature. The sample temperatures oscillate in the amplitudes of ± 0.05 K around the original. When a MW power exceeds the threshold, 0 dBm for the current study, the PID fail in the control of the sample temperatures, which increase with time, but the rising amplitudes are weaker than Case I. The ODMR lines are analogue to those of Case I. We presented in Supplemental Material the similar results for other initial sample temperatures [29].

We diagrammed in Fig. 4(c) and 4(d) the measured values of the ZFS as a function of the MW powers for Case I and II, respectively. The ZFS values of both cases appear red shifts of the MW power dependence. We are interested in the red shifts appearing with Case II for the MW powers below the threshold. As shown in Fig. 4(b), no apparent temperature rising is

recorded by the thermopile attached to the edge of the diamond sample for the MW powers below -5 dBm. Our experiment was implemented in an electromagnetic shielding room. No additional electromagnetic field was applied except for the MW fields for manipulation of the ground electronic spin triplet. The diamond sample was free from strain. We argue that the MW heating effect existed with the diamond sample even though the MW powers below the threshold. The wire antenna produced the inhomogeneous field in the sample. We can infer that the sample central is slightly hotter than the sample edge. The thermopile attached to the edge of the diamond sample missed detecting the temperature rises appearing in the central of the sample. The PID acts according to the edge temperature measured by the thermopile. Thus, the temperatures indicated by the thermopile were lower than those in the sample central region. We observed the intensified MW field in the sample central region pictured by an infrared camera [24]. The previous experimental observations support such a reasoning.

Acosta, *et al.* and others ascribe the thermal expansion responsible for the ZFS temperature dependence [5]. Doherty, *et al.* stated that the model based on pure thermal expansion dose not well describe the ZFS temperature dependence [31]. The atomic displacement arising from thermal expansion and the lattice vibration shall be both responsible for the temperature dependence of the ZFS. Tang, *et al.* indicated that the atomic thermal expansion affects negligibly the shift of the ZFS [32]. The atomic vibration around the equilibrium positions caused by phonon excitations at finite temperature dominates the ZFS shifts of temperature dependence. The phonon occupation number affects the phonon effect. Cambria, *et al.* inferred that, for the spin triplet of NV⁻ centers, changes in temperature affect the positions of atoms in the diamond lattice which in turn modulate the electronic wavefunction [33]. The ZFS shifts of temperature dependence are proportion to the occupation numbers of two representative phonon modes. Tang, *et al.* and Cambria, *et al.* share the common point that the phonon modes dominate the ZFS shifts of temperature dependence. Gali state that, as the electron spin density is highly localized to the three carbon atoms adjacent to the vacancy, the ZFS can be accurately modelled by accounting for the temperature-dependent positions of the atoms nearest the defect [34]. Therefore, we ascribe in this paper the observed red shifts to the additional vibration with the diamond lattice excited by the MW fields.

Fig. 4(c) and 4(d) show that the lower MW power brings the smaller red shift effect in the expense of the larger error bars of the values of the ZFS and the more inferior contrasts of the ODMR lines. For Case I, the random errors for the measured ZFS values, measured by the standard deviations, are in the range of 87 kHz to 413 kHz at the MW power of -25 dBm. In contrast, the measurements with the MW power of -5 dBm result in the standard deviations of 10 kHz to 61 kHz for the measurements of the ZFS and the red shifts of 294 kHz to 574 kHz in comparison with that at -25 dBm. The result implies that a high MW power brings small standard deviations of the ZFS values in the expense of the substantial red shifts of the ZFS. The analogue phenomenon occurs for Case II. Fig.4(d) shows the random errors for the measured ZFS values are in the range of 118 kHz to 364 kHz at the MW power of -25 dBm. Besides, the values of the ZFS for Case I differ from those for Case II in 47 kHz to 1505 kHz in the entire experimental range.

We observe that the plots in Fig.4(c) and 4(d) conforming to the similar asymptotic behavior of the MW power dependence. The phenomenon indicates that the red shifts asymptotically disappear with decreasing MW power. Thus, zero MW irradiation shall cast no

perturbation on the ZFS of the NV⁻ centers in diamond. The observation inspires us to form an exponential asymptotic fit of the values of the ZFS relating to the MW powers. Denote the MW power by Q in the unit of dBm, the ZFS by D in the unit of MHz. Taking into account the MW power as the free variable, we tested the exponential asymptotic fit,

$$D = a \times 10^{Q/20} + b. \quad (1)$$

We pictured the fits in Fig. 5(a) and 5(b) for Case I and II, respectively. Eq. (1) well fits D and Q . After, we converted the free variable Q into Q_1 in the unit of mW ($Q_1=10^{Q/10}$), where Table I gives the respective conversion for all the MW powers.

TABLE I. Unit conversion of the microwave power.

Q (dBm)	Q_1 (mW)	$x=Q_1^{1/2}$
-25	0.003162278	0.056234133
-20	0.01	0.1
-15	0.031622777	0.177827941
-11	0.079432823	0.281838293
-10	0.1	0.316227766
-5	0.316227766	0.562341325
0	1	1
5	3.16227766	1.77827941
6	3.981071706	1.995262315

Assuming $x=Q_1^{1/2}$, the exponential fit is then converted into the linear fit,

$$D = ax + b. \quad (2)$$

We pictured the linear fits in Fig. 5(c) and 5(d) for Case I and II, respectively. By the linear fits, the intercept b accounts for the value of the ZFS at zero MW irradiation, the unperturbed value of the ZFS.

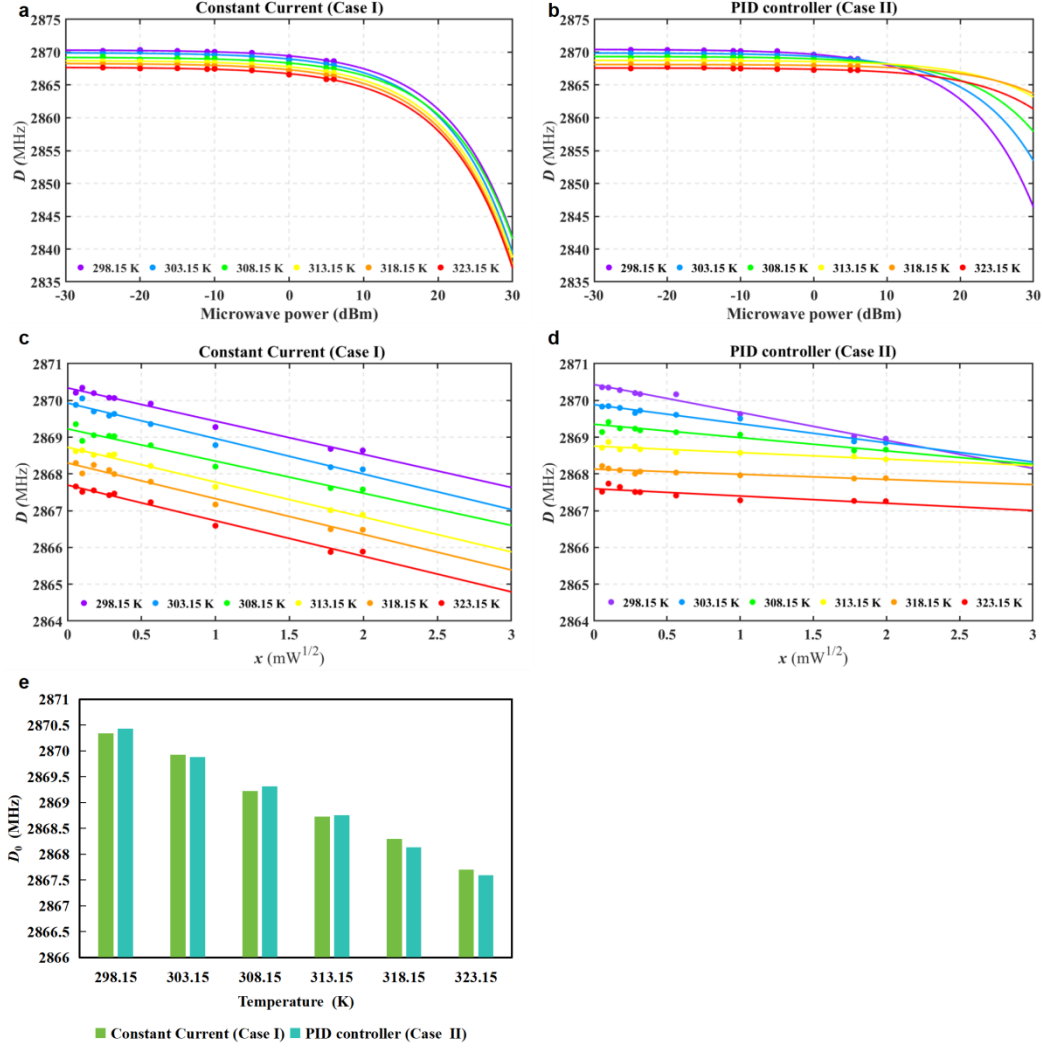


FIG. 5. (a, b) Exponential asymptotic fitting of the values of the ZFS measured at variant temperatures. (c, d) Transformation of (a, b) to linear fitting of the values of the ZFS. (e) Comparison of the intercepts of zero MW field.

Upon the fact of no red shift occurring in the absence of MW irradiation, we infer that the intercept of a single linear fit approximates the value of the ZFS of zero red shift. Thus, we argue that the intercepts of the two cases should be equal for an identical initial thermal equilibrium state of the sample. The practical difference shall denote the measurement uncertainty using the ensemble NV^- centers presented in our experiment. Accordingly, we compared in Fig. 5(e) the intercepts of the fits against the sample initial temperatures. The differences randomly vary from 29 kHz to 166 kHz over the entire experiment range. The standard deviation of the variations is 49 kHz. Given the normal distribution among the differences, the standard deviation accounts for the standard uncertainty measuring the ZFS. We stated in the previous section the red shift effect, which is responsible for the large differences of 47 kHz to 1505 kHz for the measured ZFS values between Case I and Case II.

Thus, the asymptotic approximation largely depressed the red shift effect in the entire experiment range.

The authors acknowledge the financial support by the Fundamental Research Program of the National Institute of Metrology, China (no. AKYZD2209-1, AKYRC2303, and AKYRC2301).

Corresponding author:
zhangjint@nim.ac.cn

- [1] M. W. Doherty, N. B. Manson, P. Delaney, F. Jelezko, J. Wrachtrup, L. C. L. Hollenberg, The nitrogen-vacancy colour centre in diamond. *Phys. Rep.* **528**, 1-45 (2013).
- [2] V.V. Dobrovitski, G.D. Fuchs, A.L. Falk, C. Santori, D.D. Awschalom, Quantum Control over Single Spins in Diamond. *Annu. Rev. Condens. Matter Phys.* **4**, 23-50 (2013).
- [3] R. Schirhagl, K. Chang, M. Loretz, C. L. Degen, Nitrogen-Vacancy Centers in Diamond: Nanoscale Sensors for Physics and Biology. *Annu. Rev. Phys. Chem.* **65**, 83-105 (2014).
- [4] A. Gruber, A. Dräbenstedt, C. Tietz, L. Fleury, J. Wrachtrup, C. von Borczyskowski, Scanning Confocal Optical Microscopy and Magnetic Resonance on Single Defect Centers. *Science*. **276**, 2012-2014 (1997).
- [5] V. M. Acosta, A. Jarmola, E. Bauch, D. Budker, Optical Properties of the Nitrogen-Vacancy Singlet Levels in Diamond. *Phys. Rev. B.* **82**, 201202 (2010).
- [6] G. Kucsko, P. C. Maurer, N. Y. Yao, M. Kubo, H. J. Noh, P. K. Lo, H. Park, and M. D. Lukin, Nanometre-scale thermometry in a living cell. *Nature* **500**, 54-59 (2013).
- [7] D. M. Toyli, D. J. Christle, A. Alkauskas, B. B. Buckley, C. G. Van de Walle, D. D. Awschalom, Measurement and Control of Single Nitrogen-Vacancy Center Spins above 600 K. *PNAS* **110**, 8417 – 8421 (2013).
- [8] P. Neumann, I. Jakobi, F. Dolde, C. Burk, R. Reuter, G. Waldherr, J. Honert, T. Wolf, A. Brunner, J. Wrachtrup, J. H. Shim, D. Suter, H. Sumiya, J. Isoya, High precision nano scale temperature sensing using single defects in diamond. *Nano Lett.* **13**, 2738 (2013).
- [9] D. A. Simpson, E. Morrisroe, J. M. McCoe, A. H. Lombard, D. C. Mendis, F. Treussart, L. T. Hall, S. Petrou, L. C. L. Hollenberg, Non-Neurotoxic Nanodiamond Probes for Intraneuronal Temperature Mapping. *ACS Nano.* **11**, 12077–12086 (2017).
- [10] S. Sotoma, C. X. Zhong, J. C. Y. Kah, H. Yamashita, T. Plakhotnik, Y. Harada, M. Suzuki, In situ measurements of intracellular thermal conductivity using heater - thermometer hybrid diamond nanosensor. *Sci. Adv.* **7**, eabd7888 (2021).
- [11] M. Fujiwara, S. Sun, A. Dohms, A. Dohms, Y. Nishimura, K. Suto, Y. Takezawa, K. Oshimi, L. Zhao, N. Sadzak, Y. Umehara, Y. Teki, N. Komatsu, O. Benson, Y. Shikano, E. K. Nakadai, Real-time nanodiamond thermometry probing in vivo thermogenic responses. *Sci. Adv.* **6**, eaba9636 (2020).
- [12] G. Petrini, G. Tomagra, E. Bernardi, E. Moreva, P. Traina, A. Marcantoni, F. Picollo, K. Kvaková, P. Cíglér, I. P. Degiovanni, V. Carabelli, M. Genovese, Nanodiamond - Quantum Sensors Reveal Temperature Variation Associated to Hippocampal Neurons Firing. *Adv. Sci.* **9**, 2202014 (2022).

- [13] Y. Wu, T. Weil, Recent Developments of Nanodiamond Quantum Sensors for Biological Applications. *Adv. Sci.* **9**, 2200059 (2022).
- [14] T. Zhang, G. Pramanik, K. Zhang, M. Gulka, L. Wang, J. Jing, F. Xu, Z. Li, Q. Wei, P. Cigler, Z. Chu, Toward Quantitative Bio-sensing with Nitrogen-Vacancy Center in Diamond. *ACS Sens.* **6**, 2077 – 2107 (2021).
- [15] J. F. Barry, J. M. Schloss, E. Bauch, M. J. Turner, C. A. Hart, L. M. Pham, R. L. Walsworth, Sensitivity optimization for NV-diamond magnetometry. *Rev. Mod. Phys.* **92**, 015004(68) (2020).
- [16] L. Rondin, J. P. Tetienne, T. Hingant, J. F. Roch, P. Maletinsky, V. Jacques, Magnetometry with nitrogen-vacancy defects in diamond. *Rep. Prog. Phys.* **77**, 056503 (2014).
- [17] M. Loretz, T. Roskopf, C. L. Degen, Radio-Frequency Magnetometry Using a Single Electron Spin. *PRL.* **110**, 017602 (2013).
- [18] T. de Guillebon, B. Vindolet, J. F. Roch, V. Jacques, L. Rondin, Temperature dependence of the longitudinal spin relaxation time T_1 of single nitrogen-vacancy centers in nanodiamonds. *Phys. Rev. B.* **102**, 165427 (2020).
- [19] T. Staudacher, F. Shi, S. Pezzagna, J. Meijer, J. Du, C. A. Meriles, F. Reinhard, J. Wrachtrup, Nuclear Magnetic Resonance Spectroscopy on a (5-Nanometer)³ Sample Volume. *Science.* **339**, 561-563 (2013).
- [20] M. L. Goldman, A. Sipahigil, M. W. Doherty, N. Y. Yao, S. D. Bennett, M. Markham, D. J. Twitchen, N. B. Manson, A. Kubanek, M. D. Lukin, Phonon-Induced Population Dynamics and Intersystem Crossing in Nitrogen-Vacancy Centers. *PRL.* **114**, 145502 (2015).
- [21] S. E. Lillie, D. A. Broadway, N. Dontschuk, S. C. Scholten, B. C. Johnson, S. Wolf, S. Rachel, L. C. L. Hollenberg, J. P. Tetienne, Laser Modulation of Superconductivity in a Cryogenic Wide-field Nitrogen-Vacancy Microscope. *Nano Lett.* **20**, 1855–1861 (2020).
- [22] S. M. Blakley, A. B. Fedotov, J. Becker, N. Altangerel, I. V. Fedotov, P. Hemmer, M. O. Scully, A. M. Zheltikov, Stimulated fluorescence quenching in nitrogen – vacancy centers of diamond: temperature effects. *Optics Lett.* **41**, 2077-2080 (2016).
- [23] K. Ouyang, Z. Wang, L. Xing, X. J. Feng, J. T. Zhang, C. Ren, X. T. Yang, Temperature dependence of the zero-field splitting parameter of nitrogen-vacancy centre ensembles in diamond considering microwave and laser heating effect. *Meas. Sci. Technol.* **34**, 015102 (2023).
- [24] Z. Wang, J. T. Zhang, X. J. Feng, L. Xing, Microwave Heating Effect on Diamond Samples of Nitrogen Vacancy Centers. *ACS Omega.* **7**, 31538-31543 (2022).
- [25] M. Fujiwara, Y. Shikano, Diamond quantum thermometry: from foundations to applications. *Nanotechnology.* **32**, 482002(23pp) (2021).
- [26] N. Wang, G. Q. Liu, W. H. Leong, H. Zeng, X. Feng, S. H. Li, F. Dolde, H. Fedder, J. Wrachtrup, X. D. Cui, S. Yang, Q. Li, R. B. Liu, Magnetic Criticality Enhanced Hybrid Nanodiamond Thermometer under Ambient Conditions. *Phys. Rev. X.* **8**, 011042 (2018).
- [27] J. F. Barry, M. J. Turner, J. M. Schloss, D. R. Glenn, Y. Song, M. D. Lukin, H. Park, R. L. Walsworth, Optical magnetic detection of single-neuron action potentials using quantum defects in diamond. *PNAS.* **113**, 14133-14138 (2016).
- [28] J. M. Schloss, J. F. Barry, M. J. Turner, R. L. Walsworth, Simultaneous Broadband Vector Magnetometry Using Solid-State Spins. *Phys. Rev. Applied.* **10**, 034044 (2018).
- [29] See Supplemental Material for additional experimental details

- [30] M. W. Doherty, F. Dolde, H. Fedder, F. Jelezko, J. Wrachtrup, N. B. Manson, L. C. L. Hollenberg, Theory of the ground-state spin of the NV^- center in diamond. *Phys. Rev. B.* **85**, 205203 (2012).
- [31] M. W. Doherty, V. M. Acosta, A. Jarmola, M. S. J. Barson, N. B. Manson, D. Budker, L. C. L. Hollenberg, Temperature shifts of the resonances of the NV^- center in diamond. *Phys. Rev. B.* **90**, 041201(5) (2014).
- [32] H. Tang, A. R. Barr, G. Q. Wang, P. Cappellaro, J. Li, First-Principles Calculation of the Temperature-Dependent Transition Energies in Spin Defects. *J. Phys. Chem. Lett.* **14**, 3266–3273 (2023).
- [33] M. C. Cambria, G. Thiering, A. Norambuena, H. T. Dinani, A. Gardill, I. Kemeny, V. Lordi, Á. Gali, J. R. Maze, S. Kolkowitz, Physically motivated analytical expression for the temperature dependence of the zero-field splitting of the nitrogen-vacancy center in diamond. *Phys. Rev. B.* **108**, L180102 (2023).
- [34] Á. Gali, Ab initio theory of the nitrogen-vacancy center in diamond. *Nanophotonics.* **8**, 1907-1943 (2019).